



Full Text View

[Volume 30, Issue 10 \(October 2000\)](#)

Journal of Physical Oceanography

 Article: pp. 2610–2626 | [Abstract](#) | [PDF \(321K\)](#)

Climate Variability of the Equatorial Thermocline Inferred from a Two-Moving-Layer Model of the Ventilated Thermocline^{*}

Rui Xin Huang and Joseph Pedlosky

Department of Physical Oceanography, Woods Hole Oceanographic Institutions, Woods Hole, Massachusetts

(Manuscript received June 7, 1999, in final form December 8, 1999)

DOI: 10.1175/1520-0485(2000)030<2610:CVOTET>2.0.CO;2

ABSTRACT

A two-moving-layer model is used to examine the structure of the equatorial thermocline and its connection with the extratropical thermocline. It is found that cooling (warming) in extratropics generates a low (high) potential vorticity anomaly and induces downward (upward) movement of the thermocline, and the perturbation propagates to the equatorial thermocline, inducing a downward (upward) movement of the thermocline and intensification (weakening) of the undercurrent. Thus, surface cooling in the extratropics can induce warming of the equatorial thermocline. In addition, the total mass flux in the subsurface layer in the extratropics and the equatorial undercurrent is enhanced. Although in the extratropics perturbations generated by localized cooling (warming) are confined within the characteristic cone, defined by the unperturbed trajectories of the thermocline circulation, when these perturbations propagate into the equatorial region they are no longer confined by the characteristic cone in the meridional direction.

1. Introduction

Climate variability in the equatorial regions has a profound influence on the global climate. Among other variables, sea surface temperature is probably the most important one in controlling the climate. In fact, sea surface temperature is the only oceanic parameter that can affect the atmosphere directly. Along the equator there is a strong zonal gradient of the sea surface temperature because the prevailing easterly winds push warm water toward the western boundary, and the warm water piles up at the western boundary and creates a warm water pool there. In the eastern equatorial ocean the easterlies induce equatorial upwelling of cold water, thus creating a cold water tongue near the eastern boundary. This east–west gradient in surface temperature is associated with the slope in steric sea level difference and the depth of the thermocline. Such a difference in the thermocline depth also plays a major role in the sea surface

Table of Contents:

- [Introduction](#)
- [Model formulation and](#)
- [Climate variability of](#)
- [Conclusions](#)
- [REFERENCES](#)
- [FIGURES](#)

Options:

- [Create Reference](#)
- [Email this Article](#)
- [Add to MyArchive](#)
- [Search AMS Glossary](#)

Search CrossRef for:

- [Articles Citing This Article](#)

Search Google Scholar for:

- [Rui Xin Huang](#)
- [Joseph Pedlosky](#)

temperature balance. For example, near the eastern boundary the depth of the thermocline is shallow; upwelling of cold water from the shallow base of the thermocline is a major contributor in setting up the low sea surface temperature there. Therefore, the depth of the equatorial thermocline is a very important parameter in controlling the sea surface temperature distribution in the equatorial oceans.

In particular, the zonal gradient of the thermocline depth may play a vital role in controlling the growth rate of the ocean-atmosphere coupled modes. Over the past decade many simple models have been used successfully to predict the climate anomaly associated with ENSO. However, most of these models are based on a simple multilayer assumption, in which the layer thickness is taken as the climatological mean from existing data. Thus, these models do not include the possible changes in the basic stratification of the tropical oceans due to climate change on decadal timescale. As a result, these simple multilayer models may not be able to simulate ENSO phenomenon under climate conditions different from that inferred from a climatological mean dataset.

The equatorial thermocline is certainly not set by the local dynamics; instead, it is the result of water mass formation and transformation on the global scale. Given the global thermohaline circulation and its associated water mass formation and conversion, the thermocline structure at a given location is controlled by the wind-driven circulation in the upper ocean. In particular, subduction is a major mechanism for water mass transport in the upper ocean.

This link has been explored by many investigators in the past. Many simple analytical models have been proposed in order to explain the equatorial thermocline. In some of these early theories, such as [Charney \(1960\)](#), friction plays an important role, so the solution is quite sensitive to the frictional parameterization. This connection was not clearly understood at that time.

On the other hand, study of tracer distribution in the ocean clearly showed that the equatorial thermocline is closely linked to the midlatitude thermocline (e.g., [Fine et al. 1981, 1987](#)). Furthermore, studies in the 1980s showed that friction and mixing may be unimportant for the lowest-order balance of the equatorial currents (e.g., [Bryden and Brady 1985](#)). Thus, it seemed better to interpret the equatorial currents in terms of inertial boundary layer theory ([Pedlosky 1987, 1996](#)). Since then numerous illuminating numerical models (e.g., [McCreary and Lu 1994; Lazar et al. 1999](#)), more realistic than the simple analytical model of Pedlosky, have described the linkage between the midlatitude and equatorial regions.

This connection is an important element of the global circulation. For example, [Gu and Philander \(1997\)](#) proposed that this link between the subtropics and Tropics may play a vitally important role in setting up the decadal variability of ENSO. A recent study by [Johnson and McPhaden \(1999\)](#) gave a clear three-dimensional picture of this communication window. There have been also some studies devoted to climate variability in the equatorial thermocline, such as [Deser et al. \(1996\)](#) and [Zhang et al. \(1998\)](#).

Since climate variability in the equatorial region is closely related to the structure of the equatorial thermocline, it is desirable to study the variability of the equatorial thermocline using a simple analytical model of the ventilated thermocline. Another major difficulty in dealing with the climate variability is the complicated nature of the waves involved in any time-dependent problem. Although there are comprehensive theories about the wave dynamics in the equatorial region, the corresponding theories about the wave dynamics for the extratropical region are still in an early stage of development.

We have adapted a much more modest approach in this study by examining the difference between two steady states of the thermocline structure. As in [Huang and Pedlosky \(1999\)](#) we ignore the short time response to climate perturbations that manifests itself as a largely wavelike anomaly propagation and allow the new state to come into a new equilibrium and consider the anomaly as the difference of steady states. Since the adjustment time for the first baroclinic mode is less than 10 years at low latitudes, climate variability at low latitudes on a decadal timescale may be treated as the difference between two steady states. This has the great advantage of allowing a clear analytical approach to the nonlinear problem and concentrates on the progression of the anomaly as a consequence of advection by the general circulation in both midlatitudes and the equatorial zone. Therefore, the problem of exploring the climate variability is reduced to calculating the different steady states and extracting the variability by simply subtracting one steady state from another. This approach does indeed greatly simplify our task, and we have obtained much useful information about the climate variability in the equatorial thermocline. Our approach is, of course, rather limited; however, we hope results from such a simple model may help us to understand the complicated climate phenomena directly related to the equatorial thermocline.

This paper is organized as follows: The model formulation is presented in [section 2](#), including the numerical technical details of the shooting method used in this study. The main results from our study are presented in [section 3](#), and finally our conclusions are discussed in [section 4](#).

2. Model formulation and the basic state

The ocean is represented by a two-moving-layer model, in which the water is assumed an ideal fluid, that is, without

friction and interfacial mass and momentum exchange. The model consists of two submodels: a model for the extratropical thermocline and a model for the equatorial thermocline. The theoretical backgrounds for these two submodels have been discussed in detail by [Luyten et al. \(1983\)](#) and [Pedlosky \(1996\)](#). Note that our discussion in this study is confined to the Northern Hemisphere, assuming that the equatorial thermocline and undercurrent are symmetric with respect to the equator.

Throughout, we assume that the dynamics is that of an ideal fluid that conserves potential vorticity and, in the steady state, the Bernoulli function. Thus,


$$\mathbf{u}_n \cdot \nabla q_n = 0 \quad (1a)$$

$$\mathbf{u}_n \cdot \nabla B_n = 0, \quad (1b)$$

where the subscript n labels the layer. We consider such a model as an attempt for both the thermocline and the equatorial undercurrent (EUC) in the nature of a null hypothesis with regard to vertical mixing. That is, we attempt to see how much of the structure of the midlatitude and equatorial thermocline can be explained on the basis of ideal fluid theory. This is of course not the only legitimate point of view. Numerical experiments (e.g., [Blanke and Raynaud 1997](#); [Lu et al. 1998](#)) require mixing for numerical reasons and suggest the possible importance of mixing for the dynamics. We do not consider the issue as settled and believe it is important to investigate the consequences of the ideal-fluid theory. Indeed, in our opinion the early theoretical work on the nature of the EUC (e.g., [Charney 1960](#)) depended in an oversensitive manner on the degree and nature of the vertical mixing parameterization and we attempt to remove that sensitivity with our ideal-fluid model.

In the extratropics the potential vorticity can be approximated in terms of the planetary potential vorticity, that is, $q_n = f/h_n$, while in the equatorial region the relative vorticity supplements the planetary vorticity. Since the strong currents there are zonal and very narrow, the semigeostrophic approximation leads to a representation of potential vorticity in the equatorial zone as

$$q_n = \frac{f - \partial u_n / \partial y}{h_n}.$$

Similarly, the Bernoulli function in midlatitudes is given by the pressure field in each layer that, with the hydrostatic relation, can be related to the layer thicknesses. In the equatorial region the pressure field is supplemented by the kinetic energy associated with the zonal velocity to form the Bernoulli function. The solutions in the two regions are joined together in a matching domain at the edge of the equatorial zone. The details of the dynamics in the individual regions is described by [Luyten et al. \(1983\)](#) and by [Pedlosky \(1996\)](#). [Figure 1](#)  shows a sketch of the two regions. Since the solution in the equatorial region must be computed numerically, the matching between the two regions is carried out at a latitude chosen to lie outside the EUC but close enough to the equator to respect the boundary layer character of the solution. The solution's character does not depend strongly on the latitude chosen for matching.

In the extratropics the structure of the thermocline is described in terms of a two-moving-layer model of the ventilated thermocline. Assume that the outcrop line is a zonal circle y_{out} where the Coriolis parameter is f_{out} . North of the outcrop line there is only one moving layer, and the solution is well known. Since this part of the circulation is not our concern in this study, we omit the discussion of it. South of the outcrop line there are two moving layers and the total layer depth, H_0 , obeys

$$H_0^2 = \frac{D_0^2 + H_e^2}{1 + \frac{\gamma_1}{\gamma_2}(1 - f/f_{\text{out}})^2} \quad (2)$$

where

$$\begin{aligned} D_0^2(x, y) &= -\frac{2f^2}{\gamma_2\beta} \int_{\lambda}^{\lambda_e} w_e R \cos\phi \, d\lambda' \\ &= -\frac{2}{\gamma_2} \int_{\lambda}^{\lambda_e} P_r R \cos\phi \, d\lambda', \end{aligned} \quad (3)$$

γ_1 and γ_2 are reduced gravity across the upper and lower interface, $\beta = R^{-1}df/d\Phi$, R is the radius of the earth, Φ is latitude, and P_r is the pumping rate defined as

$$P_r = \tan\Phi \tau^\lambda_\Phi - \tau^\lambda, (4)$$

where the wind stress, τ^λ , has been assumed to be strictly zonal and subscript Φ denotes differentiation. For convenience, we will assume $\gamma_1 = \gamma_2 = 1 \text{ cm s}^{-2}$ and $H_e = 0$ in this study. The second assumption is used to avoid the complication introduced by the shadow zone, and the dynamical role of the shadow zone is left for future study.

The corresponding thickness for upper and lower layers are

$$h_1 = H_0(1 - f/f_{\text{out}}), \quad h_2 = H_0 f/f_{\text{out}}. (5)$$

Assuming that the equatorial boundary current is matched with the interior solution along a latitudinal circle, $y = y_m$, where the Coriolis parameter is f_m , then the matching conditions for the interfacial depths are

$$H_0 = D_0[1 + (1 - f_m/f_{\text{out}})^2]^{-1/2}; \quad (6)$$

$$h_1 = H_0(1 - f_m/f_{\text{out}}). \quad (7)$$

The equatorial thermocline is described in terms of a two-moving-layer model (Pedlosky 1987, 1996). The major difference between the equatorial thermocline and the extratropical thermocline is that the Coriolis parameter vanishes near the equator; thus, geostrophy is no longer the dominating balance near the equator. Instead, the relative vorticity must play an important role in the dynamic balance of the equatorial undercurrent. Scaling analysis leads to a simple semigeostrophic model for the equatorial undercurrent and the thermocline. The equatorial thermocline can be described in terms of the total layer depth (h) and the zonal velocity in the second layer (u):

$$\gamma_2 h_y = -fu; \quad (8)$$

$$u_y = f - f(y_{\text{out}}) \frac{h - h_1}{\gamma_2 h + u^2/2}. \quad (9)$$

These balances assume that water flowing from the subtropics to the Tropics conserves both potential vorticity and Bernoulli function. The dependence of the potential vorticity on the Bernoulli function, $\gamma_2 h + u^2/2$, is determined by matching to the ventilated thermocline. This system of first-order differential equations is subject to the following boundary conditions: First, the lower interface depth should match that of the interior solution along the matching latitude y_m ,

$$h = H_0 \quad \text{at } y = y_m. (10)$$

Second, the equator is assumed to be a streamline so that the Bernoulli function should be a constant along the equator,

$$\gamma_2 h + \frac{u^2}{2} = B_0 \quad \text{at } y = 0. \quad (11)$$

Note that the upper-layer thickness is another unknown. In order to carry out the boundary layer calculation, we also need to specify an additional constraint on the upper-layer thickness. Pedlosky (1987) first assumed that h_1 is independent of latitude within the equatorial boundary layer and found some interesting solutions. Another choice is to assume that the upper-layer thickness is compensated within the equatorial region (Pedlosky 1996). This choice is based on the following idea: the geostrophic velocity in the upper layer is much smaller than that in the second layer; thus, to the lowest-order approximation the meridional pressure gradient in the upper layer is negligible compared with that in the second layer. This approximation implies that near the equator the current in the upper layer is dominated by the local wind stress. In addition, our earlier study (Huang and Pedlosky 1999) indicates that perturbations for the interior solution have a second baroclinic modelike feature; that is, the perturbations in the interior solution are also compensated (in a broader sense). Thus, using the compensation constraint seems a better choice.

Of course this specification of the depth of the upper layer is entirely arbitrary. In the original theory as described by [Pedlosky \(1987\)](#) the two extremes of specification of the upper-layer thickness, that is, either independent of y with no vertical shear across the interface or completely compensated, had little effect on the undercurrent or the depth of the equatorial thermocline. In the interest of keeping our model as simple and comprehensible as possible we retain this arbitrary, and admittedly deficient, element of the theory.

Although the specific constraint on h_1 only affects the equatorial thermocline solution slightly, our calculations in this study indicate that this seemingly minor change in the solution of the equatorial thermocline is more pronounced when the climate variability inferred from the model is the focus. Thus, we will use the following additional constraint on the upper-layer thickness:

$$h_1(x, y) = h_1(x, y_m) + h(x, y_m) - h(x, y), \quad (12)$$

where y_m is the latitude where the equatorial thermocline solution is matched with the interior thermocline solution. This is the compensated solution.

This system of ordinary differential equations is solved by a shooting method. [Pedlosky \(1987\)](#) solved this system by shooting from the matching latitude, that is, by assuming an initial value of u at the matching latitude and integrating the system toward the equator. By adjusting the initial guess of u a final solution can be found that satisfies the boundary condition (11) along the equator. However, this approach gives rise to a system that is quite stiff. Through our numerical experiments it was found that the system is easier to solve by shooting instead from the equator toward the extratropics. We assume an initial guess of $u > 0$ at the equator and calculate h , using boundary condition (11). The system can be integrated from the equator toward the matching latitude.

The model basin used in this study is 60° wide in the zonal direction and extends from the equator to 45°N , mimicking the situation in the Atlantic basin. The zonal wind stress profile used is

$$\tau^\lambda = -\cos\left(\frac{\phi}{\Delta\phi}\pi\right), \quad \Delta\phi = 50^\circ \quad (\text{dyn cm}^{-2}). \quad (13)$$

This wind stress profile produces a pumping rate that is always positive and has a local maximum at 28°N and a local minimum near the equator, [Fig. 2](#). Applying the simple ventilated thermocline theory of [Luyten et al. \(1983\)](#) leads to a typical circulation in the subtropical basin for the case with two moving layers, [Fig. 3](#).

The wind stress chosen here is very idealized; however, it serves the purpose of demonstrating the idea that the midlatitude thermocline is connected to the equatorial thermocline. Although simple analytical models based on zonally mean wind stress may have difficulty in bring the subtropical water into the equatorial regime due to the existence of the potential vorticity barrier near the intertropical convergence zone, it is readily shown that such problems can be overcome by a simple two-layer model in which a zonally dependent, realistic Ekman pumping distribution is used to force the model. Since this study is focused on some theoretical issues about the fundamental structure of climate variability in the equatorial thermocline, we will use the simple wind stress profile described by (13).

Although the layer thicknesses remain finite near the equator, the solution of [Luyten et al. \(1983\)](#) is not valid there because the Coriolis parameter vanishes near the equator and the geostrophic balance for the meridional velocity is invalid. As a result, the thermocline structure near the equator must be calculated by including the nonlinear advection terms.

Note that the model is very idealized. For example, we have used the assumption of a zero layer thickness along the eastern boundary in order to avoid the complication due to the existence of the shadow zone near the eastern boundary. Therefore, the values of different variables quoted in the following discussion should only serve as a means of understanding the physics controlling the climate variability, and these values should not be taken as the realistic values for the oceans.

In this study we will first calculate the thermocline structure and its climate variability in the extratropics, as discussed by [Huang and Pedlosky \(1999\)](#). Afterward, we will match the equatorial boundary layer solution with the extratropical solution along a fixed latitude, which is chosen as 3.6°N . In addition, we assume that the equatorial thermocline is fed by both the interior flow and the equatorward western boundary current and the equator is a streamline that corresponds to an interior streamline intersects the western boundary at 12°N . The choice of 12° as the bifurcation latitude is arbitrary in the present context but comports well with our idea of the southern extent of the subtropical gyre and is also suggested by the pertinent numerical models (e.g., [Huang and Liu 1999](#)).

McCreary and Lu (1994) suggest a rather complex determination of the bifurcation latitude. However, their analysis is limited to the case in which the outcrop line, at the origin of the streamline reaching the bifurcation point, lies in a region of easterlies. Hence we have decided on a heuristic selection of the latitude on the basis of earlier numerical work cited above.

Note that the choice of 12° as the bifurcation latitude, which we have chosen on the basis of other numerical experiments and for which no clear a priori theory exists, does not imply that this latitude is the most northern extent of the subtropical gyre that affects the equatorial zone. It is only the most northern point of influence on the western boundary of the gyre.

The basic solution for the equatorial thermocline is shown in Fig. 4, where the equatorial thermocline has a west–east tilt, varying from 20 m at the eastern boundary to 70 m at the western boundary, Fig. 4a. The equatorial undercurrent has a maximum velocity around 1.4 m s^{-1} , Fig. 4b. This strong current carries a mass flux of 4.5 Sv ($\text{Sv} \equiv 10^6 \text{ m}^3 \text{ s}^{-1}$), and the velocity core and the mass transport core are located within about 0.5° near the equator. Note that this transport accounts for only the contribution from a single hemisphere (in this case, northern). The lower interface depth remains nonzero, unlike the zero thickness inferred from a simple ventilated thermocline model excluding the inertial terms, as shown in Fig. 3b.

As a comparison, we calculate the difference between the solutions where the upper-layer thickness is compensated and uncompensated. In general, these two solutions have similar structure, with some minor differences. As shown in Fig. 5, the compensated solution has a slightly shallower thermocline along the equator, and the difference is about 10 m. Note that due to the depth compensation the second layer thickness for the compensated model is slightly larger (figure not included.) The equatorial undercurrent in the compensated solution is narrower than that of the uncompensated solution. The most noticeable difference is that along the outer edge of the equatorial undercurrent core velocity in the compensated model is about 25 cm s^{-1} slower than that of the uncompensated model, so the Bernoulli head is also slightly smaller, Fig. 5c. The compensated solution also has a slightly larger mass flux, about 0.5 Sv for the current case, Fig. 5.

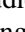

3. Climate variability of the equatorial thermocline

We have carried out a series of calculations in order to explore the variability of the equatorial thermocline induced by climate anomalies originating from the extratropics using our simple model. The seven examples discussed below have been chosen to illustrate particularly significant aspects of the coupling dynamics between midlatitude and equatorial circulation. Thus, we will consider



1. the uniform displacement of the outcrop line southward (basin-scale cooling),
2. a tilted displacement of an outcrop line (cooling in the east, warming in the west),
3. a test of the sensitivity of the solution to a different choice of bifurcation latitude,
4. a case similar to 2) where only cooling in the east is considered,
5. the response to a global anomaly in the wind stress field,
6. a similar response to a latitudinally localized wind stress anomaly,
7. a restricted region in longitude of cooling of much less than basin scale.


The variability of the extratropical thermocline in response to climate anomalies, such as cooling/warming or intensifying/weakening of Ekman pumping, has been studied in our previous paper, Huang and Pedlosky (1999). It was shown that an anomaly in the thermocline structure is most likely to appear in a second baroclinic modelike feature, and the anomaly propagates downstream from the forcing region. For example, due to surface cooling the outcrop line is displaced southward. As a result, south of the outcrop line the upper layer becomes thinner and the base of the thermocline moves downward. This signal then moves through the thermocline along trajectories described by Huang and Pedlosky (1999).



A similar phenomenon happens in the equatorial thermocline. As the outcrop line is moved from 18° to 15°N (that mimics surface cooling), the base of the thermocline moves down, reaching a maximum of 3 m along the equator, Fig. 6a. At the same time the equatorial undercurrent speeds up; the maximum change of the zonal velocity, 10 cm s^{-1} , is located about 1° off the equator and near the eastern boundary, Fig. 6b. Due to the changes in both layer depth and velocity, the Bernoulli head of the undercurrent increases substantially. The mass transport in the equatorial undercurrent increases about 1.1 Sv in response to cooling, Fig. 6d.

As the second case, shown in [Fig. 7](#) , we studied the variability induced by cooling in the eastern basin and warming in the western basin, and this is represented by moving the outcrop line to a new position, 21°N at the western boundary and 15°N at the eastern boundary. The difference between the new state and the old state (with the outcrop line along 18°N) is similar to the previous case. The major difference appears near the equator, where the thermocline depth variability is about 1.8 m, much smaller than the previous case. The intensification of the equatorial undercurrent due to this cooling/heating is smaller than the previous case. In addition, there is a narrow band right on the equator where the undercurrent slows down., [Fig. 7b](#) . The change in the Bernoulli head of the undercurrent is also smaller than the previous case. The total change in the mass flux of the second layer is reduced to about 0.6 Sv.

In general, the difference between these two cases is small, and this is due to the fact that changes in the equatorial thermocline are primarily produced through the pathway of subduction in the extratropics and thereafter movement toward the equator. Since only the streamlines stemming from a rather narrow zone near the eastern boundary can reach the equatorial region, through either the western boundary current or directly through the interior, the variability in the equatorial thermocline is controlled primarily by climate variability near the eastern boundary. Therefore, the variability in the equatorial thermocline for these two cases should be rather similar.




As the third experiment, we explore the dynamical influence of choosing a different matching condition along the equator. Specifically, we run two cases where the Bernoulli function constant along the equator was chosen as those at the western edge of the basin at 12° and 15°N respectively, [Figs. 7](#)  and [8](#) . This models the changes induced by moving the bifurcation point of the western boundary from 12° to 15°N. The variability patterns in these two case look rather similar. The only difference between these two cases is that thermocline depth variability is slightly larger (2m for the new case) and the zone where the undercurrent slows down is wider for the new case. In addition, the mass flux anomaly increases to 0.8 Sv. Therefore, our solution seems rather insensitive to the choice of the location where the western boundary current bifurcates.

In addition, we explored the dynamic impact due to changes in the wind stress forcing. As an example, when the wind stress is increased 20%, the depth of the equatorial thermocline increases, [Fig. 9](#) , and the core of the equatorial thermocline intensifies. Note that the change in the equatorial thermocline has patterns very similar to the structure of the basic state; that is, variability in the equatorial thermocline appears in the first baroclinic mode. (Note that our discussion is limited to the upper ocean defined as above the main thermocline, thus the lowest mode of variability possible is the first baroclinic mode.) In our earlier paper ([Huang and Pedlosky 1999](#)) it was shown that anomalous wind stress can induce thermocline variability in the first baroclinic mode. In addition, if the outcrop line is tilted, there is also variability appearing in a second baroclinic modelike feature. Any changes in the extratropics would affect the equatorial thermocline if the signals can reach the equatorial region through either the western boundary passage or the interior pathway.

Since only streamlines stemming from a rather narrow region near the eastern boundary can reach the equator, only a wind stress anomaly near the eastern boundary at the lower latitude may affect the equatorial thermocline. Thus, if an experiment similar to the case shown in [Fig. 9](#)  is carried out for the case when the outcrop line is tilted from 21°N at the western boundary to 15°N at the eastern boundary, a 20% increase in the wind stress over the whole basin leads to variability in the equatorial thermocline that is very similar to the results shown in [Fig. 9](#) . (The results are not included.)

On the other hand, if the wind stress anomaly is confined to a local band, the situation is different. If now,

$$\tau^\lambda = - \left\{ 1 + \exp \left[- \left(\frac{\phi - \phi_0}{\delta\phi} \right)^2 \right] \Delta w \right\} \times \cos \left(\frac{\phi}{\Delta\phi} \pi \right) \quad (\text{dyn cm}^{-2}), \quad (14)$$

where $\Delta w = 0.1$, $\phi_0 = 18^\circ$, $\delta\phi = 4^\circ$, and $\Delta\phi = 50^\circ$. This perturbed wind stress and its associated pumping rate are indicated by dashed lines in [Fig. 2](#) . As discussed by [Huang and Pedlosky \(1999\)](#), an enhanced pumping rate associated with a northwest–southeast tilted outcrop line induces variability in the thermocline similar to surface cooling. Therefore, the main thermocline moves downward in the extratropics in response to the local enhancement of the easterly wind. As a result, the equatorial thermocline also moves downward, about 18 cm. The equatorial undercurrent speeds up, 0.6 cm s^{-1} . The Bernoulli head increases, and the mass flux in the second layer increase about 0.07 Sv [Fig. 10](#) . These changes are quite similar to that induced by surface cooling, as shown in [Fig. 6](#) .

Our discussion above concerns the variability induced by basin-scale climate anomalies. It is of considerable interest to study the variability due to a localized climate anomaly. As discussed by [Huang and Pedlosky \(1999\)](#), the climate anomaly

inferred from subtracting two steady states in the extratropics propagates within the characteristics issuing from the edges of the region of anomalous forcing. These two bounding streamlines carve out a cone in the midlatitude thermocline that contains the downstream manifestation of the region of anomalous forcing. Regions outside the cone remain unaffected by the perturbation in the outcrop lines. Thus, examining longitudinally localized cooling illustrates the domains of influence of midlatitude climate perturbations. In the equatorial region, the situation is much more complicated due to the nonlinearity associated with the inertial terms in the momentum equations.

As an example, we examine the variability induced by a localized cooling. In order to show a clear picture, we have chosen a latitude rather close to the equator, $\Phi = 13.5^\circ$. The cooling is located near the eastern boundary and is in the form of an equatorward movement of the outcrop line

$$\delta\phi = \begin{cases} \Delta\Phi \left(1 - \frac{|\lambda - \lambda_0|}{\Delta\lambda}\right), & \text{if } |\lambda - \lambda_0| \leq \Delta\lambda \\ 0, & \text{otherwise,} \end{cases} \quad (15)$$

where $\Delta\Phi = -0.3^\circ$, $\lambda_0 = 58.75^\circ\text{E}$, $\Delta\lambda = 1^\circ$.

Due to the surface cooling the lower interface moves downward and the perturbations are totally confined within the characteristic cone, as discussed by [Huang and Pedlosky \(1999\)](#). For the ideal-fluid thermocline, density, potential vorticity, and Bernoulli function are conserved along streamlines; thus, perturbations are propagated along streamlines, which are called characteristics. The characteristic cone is defined by the eastmost and westmost streamlines stemmed from the edge of the area of anomalous forcing, as discussed by [Huang and Pedlosky \(1999\)](#).

The perturbations to the interfacial depth and velocity are shown in the upper part of [Figs. 11a and 11b](#). Note that the scales of the vertical coordinates are slightly different for the upper and lower parts of these figures. As required by the model formulation, the layer depth from the interior solution and the boundary layer solution do match perfectly along the matching latitude; however, the velocity in the second layer does not match exactly because it is not required as part of the matching condition, [Fig. 11b](#).

The figures overemphasize the apparent mismatch in zonal velocity as a consequence of the need to carry out the equatorial portion of the calculation numerically and for finite values of the asymptotic parameters on which the boundary layer theory for the EUC is based. This, however, presents no difficulty in determining the amplitude or vertical structure of the anomalies.



Within the equatorial thermocline, however, perturbations to the interfacial depth and velocity are no longer confined to the characteristic cone defined by the two streamlines of the unperturbed solution of the equatorial thermocline. Although the maximum of the variability appears within the characteristic cone, there are perturbations outside the cone, [Figs. 11a and 11b](#).

Anomalies formed in midlatitude by either heating or cooling are contained within characteristic cone described by [Huang and Pedlosky \(1999\)](#). This cone is formed by the potential vorticity isolines, which are identical to the trajectories in the ideal-fluid model, that issue from the edges of the zone of the perturbation. These edge trajectories or critical streamlines define the zone of perturbation in midlatitudes. The potential vorticity anomalies move along the streamlines within these cones and the perturbations in layer thickness, which in midlatitudes are algebraically related to the potential vorticity anomalies, are restricted to this region. Perturbations in velocity are similarly restricted.

The situation is different, however, in the equatorial zone. The potential vorticity anomalies are still restricted to the streamlines of the flow that emanate from the region of midlatitude heating or cooling. Now, however, in the equatorial zone the relative vorticity makes an important contribution to the potential vorticity. To obtain the layer thicknesses from a given potential vorticity anomaly, an elliptic problem for the layer thickness must be solved (the standard potential vorticity inversion). This implies, as seen in the figures, that the region affected by the potential vorticity anomalies will extend in latitude outside the core of the inertial boundary layer. This indirect influence of the heating and cooling expands the equatorial region affected by the midlatitude anomalies to a region outside the critical streamlines.

Thus, the equatorial thermocline can be classified into different dynamic domains, as shown in [Fig. 12](#), where a characteristic cone can be defined by tracking the streamlines stemming from the outer edge of the anomalous forcing in the extratropics. Here a domain of direct influence is defined by these two characteristics, and the climate anomaly within this domain can be directly linked to the anomalous forcing upstream. Near the western boundary there is a domain of silence, where no perturbation exists. Note that the domain of silence may disappear if the characteristic cone covers the whole

equatorial basin in the zonal direction, as will be shown in the next example. Near the edge of the characteristic cone is the domain of indirect influence, marked I, referring to the domain outside the critical trajectories where perturbations in layer thickness and/or velocity are found. Although the perturbations are more widely spread, the dominant effect is certainly still found within the characteristic cone.




Although the base of the equatorial thermocline moves downward in response to cooling in most parts of the equatorial basin, there is also a small region near the equator where the base of the thermocline moves upward. What is more important, the core of the equatorial undercurrent seems to slow down except for a small region in the upper edge of the characteristic cone. Changes in layer depth and velocity lead to an increase of the Bernoulli head for the outer part of the equatorial solution, but a decline in the inner core, [Fig. 11c](#) . On the other hand, these changes lead to an overall increase in the mass flux in the second layer [Fig. 11d](#) .

Another interesting case demonstrates how the cooling anomaly in the extratropics affects the equatorial thermocline through the western boundary current. The unperturbed outcrop line is along 18°N, and the cooling profile is

$$\delta\phi = \begin{cases} \Delta\Phi \left(1 - \frac{|\lambda - \lambda_0|}{\Delta\lambda}\right), & \text{if } |\lambda - \lambda_0| \leq \Delta\lambda \\ 0, & \text{otherwise,} \end{cases} \quad (16)$$

where $\Delta\Phi = -0.5^\circ$, $\lambda_0 = 55^\circ\text{E}$, $\Delta\lambda = 6^\circ$.

The cooling anomaly hits the western boundary between 5° and 9°N, so there is no perturbation reaching the equator by going through the interior. However, since we have assumed that the western boundary current bifurcates at 12°N, this anomaly should reach the equatorial region through the western boundary current. As a result, the equatorial thermocline changes in response, although there is a wide region between the equator and the extratropics where the perturbation is virtually zero.

It is interesting to note that the anomaly in equatorial thermocline depth is much smaller than that in the extratropics, [Fig. 13a](#) ; however, the perturbation in the velocity of the equatorial undercurrent is amplified, [Fig. 13b](#) . The mass flux in the second layer increases in response to cooling in the extratropics, [Fig. 13d](#) . Since the characteristic cone stems from the western boundary, the domain of silence disappears; therefore, the equatorial ocean consists of both the domain of direct influence and domain of indirect influence. Obviously, if the cooling anomaly hits the western boundary at a latitude higher than the bifurcation latitude, there would be no anomaly in the equatorial thermocline.

4. Conclusions

We have used a simple two-moving-layer model to examine the structure of the equatorial thermocline and undercurrent. It is found that climate variabilities in the equatorial thermocline share both similarity and dissimilarity with that of the extratropical thermocline.

The similarity between these two regions is that cooling (warming) in the extratropics generates low (high) potential vorticity anomaly and induces a downward (upward) movement of the thermocline. The perturbations propagate to the equatorial region and induce a downward (upward) movement of the equatorial thermocline and speed up (down) the undercurrent. Thus, surface cooling in the extratropics can induce warming of the equatorial thermocline. In addition, the total mass flux in the equatorial undercurrent is enhanced.

Anomalies formed in midlatitude by either heating or cooling are contained within characteristic cone. This cone is formed by the potential vorticity isolines, which are identical to the trajectories in the ideal-fluid model, that issue from the edges of the zone of the perturbation. These edge trajectories or critical streamlines define the zone of perturbation in midlatitudes.

The situation is different, however, in the equatorial zone. The potential vorticity anomalies are still restricted to the streamlines of the flow that emanate from the region of midlatitude heating or cooling. However, in the equatorial zone the relative vorticity makes an important contribution to the potential vorticity. To obtain the layer thicknesses from a given potential vorticity anomaly, an elliptic problem for the layer thickness must be solved. Thus the region affected by the potential vorticity anomalies will extend in latitude outside the core of the inertial boundary layer.

Our study is a first attempt to unravel the mystery of the climate variability in the equatorial thermocline induced by anomalous forcing in the extratropics. The similarity and the dissimilarity of the solutions in the extratropics and Tropics are both profound and intricate. We hope this study can stimulate further study along this line.

Acknowledgments

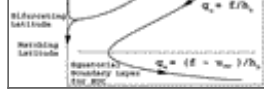
RXH was supported by the National Science Foundation through Grant OCE-9616950 and by NOAA through Grant NA96GP0460 to the Woods Hole Oceanographic Institution. JP was supported by National Science Foundation through Grant OCE-9301845 to the Woods Hole Oceanographic Institution.

REFERENCES

- Blanke, B., and S. Raynaud, 1997: Kinematics of the Pacific Equatorial Undercurrent: An Eulerian and Lagrangian approach from GCM results. *J. Phys. Oceanogr.*, **27**, 1038–1053.. [Find this article online](#)
- Bryden, H. L., and E. C. Brady, 1985: Diagnostic model of the three-dimensional circulation in the upper equatorial Pacific Ocean. *J. Phys. Oceanogr.*, **15**, 1255–1273.. [Find this article online](#)
- Charney, J. G., 1960: Non-linear theory of a wind-driven homogeneous layer near the Equator. *Deep-Sea Res.*, **6**, 303–310..
- Deser, C., M. A. Alexander, and M. S. Timlin, 1996: Upper-ocean thermal variations in the North Pacific during 1970–1991. *J. Climate*, **9**, 1840–1855.. [Find this article online](#)
- Fine, R., J. L. Reid, and H. G. Ostlund, 1981: Circulation of tritium in the Pacific Ocean. *J. Phys. Oceanogr.*, **11**, 3–14.. [Find this article online](#)
- , W. H. Peterson, and H. G. Ostlund, 1987: The penetration of tritium into the tropical Pacific. *J. Phys. Oceanogr.*, **17**, 553–564.. [Find this article online](#)
- Gu, D., and S. G. Philander, 1997: Interdecadal climate fluctuations that depend on exchanges between the tropics and extratropics. *Science*, **275**, 805–807..
- Huang, B., and Z. Liu, 1999: Pacific subtropical-tropical thermocline water exchange in the National Centers for Environmental Prediction ocean model. *J. Geophys. Res.*, **104**(C5), 11 065–11 076..
- Huang, R. X., and J. Pedlosky, 1999: Climate variability inferred from a layered model of the ventilated thermocline. *J. Phys. Oceanogr.*, **29**, 779–790.. [Find this article online](#)
- Johnson, G. C., and M. J. McPhaden, 1999: Interior pycnocline flow from the subtropical to the equatorial Pacific Ocean. *J. Phys. Oceanogr.*, **29**, 3073–3089.. [Find this article online](#)
- Lazar, A., R. Murtugudde, and A. Busalacchi, 1999: A model study of the propagation of temperature anomaly from subtropics to tropics within the southern Atlantic thermocline. *J. Geophys. Res.*, in press..
- Lu, P., J. P. McCreary Jr., and B. A. Klinger, 1998: Meridional circulation cells and the source waters of the Pacific Equatorial Undercurrent. *J. Phys. Oceanogr.*, **28**, 62–84.. [Find this article online](#)
- Luyten, J. R., J. Pedlosky, and H. Stommel, 1983: The ventilated thermocline. *J. Phys. Oceanogr.*, **13**, 292–309.. [Find this article online](#)
- McCreary, J. P., and P. Lu, 1994: Interaction between the subtropical and equatorial ocean circulations: The subtropical cell. *J. Phys. Oceanogr.*, **24**, 466–497.. [Find this article online](#)
- Pedlosky, J., 1987: An inertial theory of the equatorial undercurrent. *J. Phys. Oceanogr.*, **17**, 1978–1985.. [Find this article online](#)
- , 1996: *Ocean Circulation Theory*. Springer-Verlag, 453 pp..
- Zhang, R. H., L. M. Rothstein, and A. J. Busalacchi, 1998: Origin of upper-ocean warming and El Nino change on decadal scales in the tropical Pacific Ocean. *Nature*, **391**, 879–883..
-

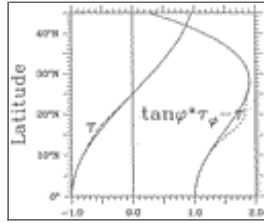
Figures





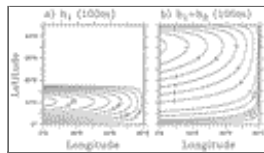
Click on thumbnail for full-sized image.

Fig. 1. Sketch of the model, where the bifurcation latitude indicates the latitude at which the western boundary current splits into the poleward and equatorward branches. The midlatitude thermocline solution and the equatorial boundary layer are matched along the matching latitude



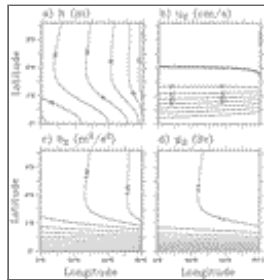
Click on thumbnail for full-sized image.

Fig. 2. Wind stress and pumping rate profiles (in dyn cm^{-2}). The dashed lines indicate the profiles used for a case with wind stress perturbation, discussed in [Fig. 10](#)



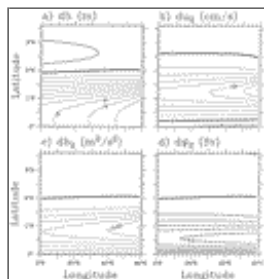
Click on thumbnail for full-sized image.

Fig. 3. Upper and lower interface depth, in 100 m. The outcrop line is along 18°N



Click on thumbnail for full-sized image.

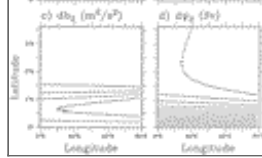
Fig. 4. Structure of the equatorial thermocline: in the extratropics the upper layer outcrops along 18°N ; the boundary layer solution matches the interior solution at 3.6°N ; the Bernoulli function is chosen at the western boundary at 12°N . (a) The lower interface depth; (b) the zonal velocity in the second layer; (c) the Bernoulli function in the second layer; (d) the streamfunction in the second layer



Click on thumbnail for full-sized image.

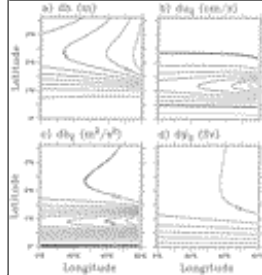
Fig. 5. Difference between the solution with the upper layer compensated and uncompensated: the boundary layer solution matches the interior solution at 3.6°N ; the Bernoulli function is chosen at the western boundary at 12°N . (a) The lower interface depth; (b) the zonal velocity in the second layer; (c) the Bernoulli function in the second layer; (d) the streamfunction in the second layer





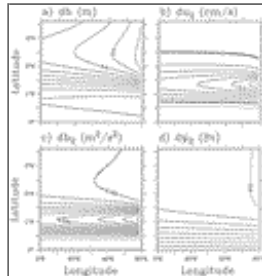
[Click on thumbnail for full-sized image.](#)

Fig. 6. Variability of the equatorial thermocline due to cooling, i.e., the outcrop line was moved from 18° to 15°N ; the boundary layer solution matches the interior solution at 3.6°N ; the Bernoulli function is chosen at the western boundary at 12°N . (a) The perturbation of the lower interface depth; (b) the perturbation of the zonal velocity in the second layer; (c) the perturbation of the Bernoulli function in the second layer; (d) the perturbation of the streamfunction in the second layer



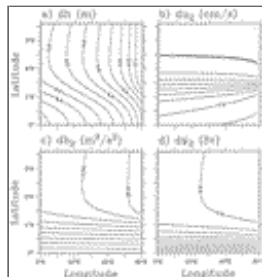
[Click on thumbnail for full-sized image.](#)

Fig. 7. Variability of the equatorial thermocline due to cooling in the eastern basin and warming in the western basin; the boundary layer solution matches the interior solution at 3.2°N ; the Bernoulli function is chosen at the western boundary at 12°N



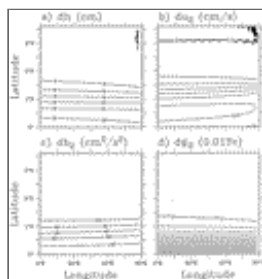
[Click on thumbnail for full-sized image.](#)

Fig. 8. Variability of the equatorial thermocline due to cooling in the eastern basin and warming in the western basin; the boundary layer solution matches the interior solution at 3.6°N ; the Bernoulli function is chosen at the western boundary at 15°N



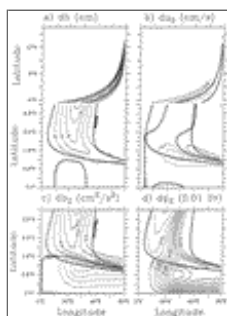
[Click on thumbnail for full-sized image.](#)

Fig. 9. Variability of the equatorial thermocline due to the 20% increase in wind stress. The first layer outcrops along 18°N , and the boundary layer solution matches the interior solution at 3.6°N ; the Bernoulli function is chosen at the western boundary at 12°N



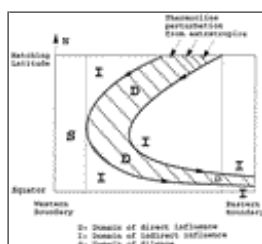
[Click on thumbnail for full-sized image.](#)

Fig. 10. Variability of the equatorial thermocline due to the 10% increase in wind stress within a local band centralized around 18°N, as depicted by the dashed line in Fig. 1. The first layer outcrops is tilted from 21°N at the western boundary to 15°N at the eastern boundary, and the boundary layer solution matches the interior solution at 3.6°N; the Bernoulli function is chosen at the western boundary at 12°N



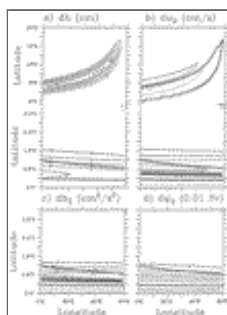
[Click on thumbnail for full-sized image.](#)

Fig. 11. Variability of the equatorial thermocline due to cooling localized within $58.25^\circ\text{E} \leq \lambda \leq 59.25^\circ\text{E}$: The outcrop line is along 13.5°N; the boundary layer solution matches the interior solution at 3.6°N; the Bernoulli function is chosen at the western boundary at 12°N. The heavy dashed lines indicate the unperturbed streamlines stemmed from the eastern and western edges of the perturbed outcrop zone in the extratropics



[Click on thumbnail for full-sized image.](#)

Fig. 12. Sketch of the different dynamic domains in the equatorial thermocline



[Click on thumbnail for full-sized image.](#)

Fig. 13. Variability of the equatorial thermocline due to cooling localized within $52^\circ\text{E} \leq \lambda \leq 58^\circ\text{E}$: The outcrop line is along 18°N; the boundary layer solution matches the interior solution at 3.6°N; the Bernoulli function is chosen at the western boundary at 12°N. The heavy dashed lines indicate the unperturbed streamlines stemmed from the eastern and western edges of the perturbed outcrop zone in the extratropics

* Woods Hole Oceanographic Institution Contribution Number 9979.

Corresponding author address: Dr. Joseph Pedlosky, Dept. of Physical Oceanography, Woods Hole Oceanographic Institution, Clark 363, MS#21, Woods Hole, MA 02543.

E-mail: jpedlosky@whoi.edu



© 2008 American Meteorological Society [Privacy Policy and Disclaimer](#)

Headquarters: 45 Beacon Street Boston, MA 02108-3693

DC Office: 1120 G Street, NW, Suite 800 Washington DC, 20005-3826

amsinfo@ametsoc.org Phone: 617-227-2425 Fax: 617-742-8718

[Allen Press, Inc.](#) assists in the online publication of *AMS* journals.